THERMO-MECHANICAL SELECTIVE LASER ASSISTED DIE TRANSFER

A Thesis
Submitted to the Graduate Faculty
of the
North Dakota State University
of Agriculture and Applied Science

By

Ross Alan Miller

In Partial Fulfillment of the Requirements
for the Degree of
MASTER OF SCIENCE

Major Department:
Electrical and Computer Engineering

May 2011

Fargo, North Dakota

North Dakota State University
Graduate School

Title

THERMO-MECHANICAL SELECTIVE LASER ASSISTED DIE TRANSFER

By

Ross A. Miller

The Supervisory Committee certifies that this ***disquisition*** complies with North Dakota State University's regulations and meets the accepted standards for the degree of

MASTER OF SCIENCE

ABSTRACT

Miller, Ross Alan, M.S., Department of Electrical and Computer Engineering, College of Engineering and Architecture, North Dakota State University, May 2011. Thermo-Mechanical Selective Laser Assisted Die Transfer. Major Professor: Dr. Ivan T. Lima, Jr.

Laser Induced Forward Transfer (LIFT) techniques show promise as a disruptive technology which will enable the placement of components smaller than what conventional pick-and-place techniques are capable of today. Limitations of current die-attach techniques are presented and discussed and present the opportunity for a new placement method. This study introduces the Thermo-Mechanical Selective Laser Assisted Die Transfer (*tm*SLADT) process and is an application of the unique blistering behavior of a dynamic releasing layer when irradiated by low energy focused UV laser pulses. The potential of *tm*SLADT as the next generation LIFT technique is demonstrated by the "touchless" transfer of 65 μm thick silicon tiles between two substrates spaced 195 μm apart. Additionally, the advantages of an enclosed blister-actuator mechanism over previously studied ablative and thermal releasing techniques are discussed. Finally, experimental results studying transfer precision indicate this non optimized die transfer process compares with, and may exceed, the placement precision of current assembly techniques.

ACKNOWLEDGEMENTS

This material is based on research sponsored by the Defense Microelectronics Activity (DMEA) under agreement number H94003-09-2-0905. The United States Government is authorized to reproduce and distribute reprints for Government purposes, notwithstanding any copyright notation thereon.

It is my pleasure to thank those that supported my efforts during the course of my studies over the last two years. The completion of this thesis would not have been possible without tremendous support and flexibility from my committee. Specifically, I would like to express my gratitude to my co-advisors Drs. Ivan Lima and Val Marinov for your generous contribution of time and insights during Project Firefly and the work presented in this thesis. To Dr. Orven Swenson, thank you for sharing your knowledge and experience and for your contributions to this thesis work. And to Dr. David Rogers, I very much appreciate your involvement in this committee; thank you for your time. Thank you Dr. Mark Pavicic and Ferdous Sarwar for your earlier contributions to the development of this laser assisted die transfer technique.

Finally, to my wife, Jaclyn, I thank you from the bottom of my heart for your patience and support while I have been a full-time student.

TABLE OF CONTENTS

LIST OF TABLES

LIST OF FIGURES

LIST OF ACRONYMS AND ABREVIATIONS

CNSE – Center for Nanoscale Science and Engineering

CPH – chips per hour

DRL – dynamic releasing layer

FSA® – Fluidic Self Assembly

HIPPO – high intensity peak-power oscillator

IC – integrated circuit

LCP – liquid crystal polymer

LED – light emitting diode

LIFT – laser induced forward transfer

MEMS – micro-electro-mechanical system

MIBK – methyl isobutyl ketone

PSA – pressure sensitive adhesive

PVC – polyvinyl chloride

RFID – radio frequency identification

*tm*SLADT – Thermo-Mechanical Laser Assisted Die Transfer

UTCP – ultra-thin chip packaging

UV – ultraviolet

DEFINITIONS

There are no industry-wide standards for many terms pertinent to semiconductor device fabrication. Following are a set of definitions to provide clarity throughout this document.

Wafer	A slice taken from a monocrystalline ingot of a semiconductor material such as silicon.
Integrated circuit (IC)	An electronic circuit manufactured on the wafer surface.
Die (pl. dice)	A part of the wafer containing a completed and autonomous integrated circuit.
Bare die	Die that has been cut out from the wafer and is ready for packaging.
Chip	A bare die packaged in a plastic encasement.
Tile	Analogous to bare die but is fabricated from a wafer containing no circuitry – strictly used for evaluating die placement techniques.

1. INTRODUCTION

The integration of materials science with electronics manufacturing techniques has provided polymer-based flex substrate materials with mechanical properties which provide excellent pairing with thin semiconductor components. Ultimately, Ultra-Thin Chip Packaging (UTCP) is an interesting field of research as the possibility of delivering conformal, wearable and, in some cases, even disposable microelectronic devices will revolutionize the way technology integrates into our lives. These devices have the potential to enhance our security, make commerce more efficient, enable new capabilities in healthcare and potentially will provide consumer electronics users the opportunity to integrate computing into their daily lives like never before. All this will be made possible by the ability of flex substrate devices to bend, roll, and fold into complex geometries. They will also provide the capability for ultra-thin 3D modules that result from stacking or other combinations of multiple flexible devices. Most proposed UTCP fabrication methods fall into one of these three categories: (i) die flip chip bonded onto flex, (ii) die laminated onto liquid crystal polymer (LCP) films, or (iii) die embedded in polyimide [1-8]. The embedded flexible silicon technology has been and is still being actively developed mostly in Europe, especially by the Fraunhofer group in Germany [9]. As a result of these capabilities and packaging techniques, devices can be integrated into documents, products or placed on nearly any type of object or device for, seemingly, infinite applications.

The use of bare dice in flexible circuits introduces an additional set of requirements including reduced footprint, low profile and flexibility of the silicon compatible to that of the polymer substrate. These factors mandate that bare dice must be flexible in the next generation of RFID tags, electronic labels, bank cards, and other low-cost disposable

electronic devices typically packaged on a flexible substrate [9] as well as in the traditionally tightly packaged conformal flexible circuits such as those used in, for example, portable consumer electronics. The bulk material properties of commonly used semiconductors, specifically, crystalline Si, make it rigid and brittle. However, thin Si behaves differently because the internal stress induced by bending, to a point, is below the fracture limit. When Si is thinned to 50 μm or less it becomes much more pliable and is thus suited for embedding into thin flex substrates [4], and the thinner the Si the more flexible it becomes. Fragile yet flexible enough, the ultra-thin bare dice provide the flexibility required for these applications [2]. The implantation of flexible components into a substrate allow the entire device to bend and flex uniformly like one homogeneous material. The use of thinned Si devices also provides the advantage of reducing the parasitic influences of Si which is especially advantageous for high frequency (GHz) devices [6]. In addition to the unique functionality provided by UTCP, reduced die size provides a cost savings; smaller dice mean higher throughput from the wafer, ergo, less cost per die. Thinner wafers mean more slices from the ingot, thus, reducing the material cost even further.

The fabrication of semiconductor devices is generally referred to by two high-level processes known as front-end and back-end processing [10]. Front-end refers to the wafer-level processing that begins with a bare wafer and generally includes various sequences of wafer doping, photolithography, etching, metallization, surface passivation, and back-lapping or wafer thinning. Back-end refers to the processing that occurs after front-end processing and includes IC dicing, die placement, and die-attach processes. This study focuses on back-end electronics packaging techniques.

In the back-end processing sequence the size of the bare die is limited by two factors: the substrate interconnect technology and die handling techniques. For the same circuit functionality (i.e., the same number of I/Os), reducing the die size means ultrafine-pitch, high-density dice with pitches of 70 μm or less for peripheral and 100 μm or less for area array pad configurations. The small pitch presents a clear challenge to the substrate technologies. Fine resolution, high interconnect density flexible substrates are possible by a number of technologies, but their cost may be prohibitive for low-cost, disposable electronics. Solutions involve the use of interconnect technologies designed to address the mismatch in the resolutions achievable by the front-end thin-film IC fabrication technology and those typical for the thick-film substrates, without compromising the production cost [11].

This thesis presents the principles of a laser-assisted bare die placement technique developed at NDSU's Center for Nanoscale Science and Engineering (CNSE) in Fargo, ND, for contactless assembly of ultra-thin bare dice onto various rigid and flexible substrates. This technology can be used for flip chip surface bonding of bumped dice or for embedding of thinned dice in the substrate as well as several other similar applications such as MEMS assembly and processing.

2. LITERATURE SURVEY – CURRENT DIRECT CHIP ATTACH TECHNIQUES

2.1. Pick-and-Place

Direct chip attach refers to the process by which bare die components are directly placed and bonded to a substrate. Currently, there is no satisfactory technique for handling ultra-thin (< 50 μm thick) bare dice. These dice are very fragile and tend to be easily damaged by the pick-and-place equipment conventionally used for direct chip attach [12, 13]. The chip shooter machines in use today [14, 15] work by picking up bare dice from carrier tape with a vacuum nozzle. The machine then positions the die at the desired location and places it on the substrate. The placement head down-force upon pickup allows for the vacuum nozzle to attain a seal on the component. The analogous force upon placement is used to establish contact between the flip chip bumps, which are generally on the component to begin with, and the substrate contacts. Placement accuracy and rate for these types of machines are inversely correlated. According to Gilleo [16], the most advanced single nozzle placement machines are capable of 4σ placement accuracies of ± 15 μm at a rate of 2000 components per hour (cph). Multiple nozzle placement machines are capable of up to 100,000 cph but with 4σ placement accuracy degraded to ± 100 μm.

For components smaller than 300 μm, stiction issues are a near certainty [17]. The small forces observed on surfaces, such as Van der Waals, surface tension, and electrostatic forces do not need to be considered for large-scale components. However, when components reduce to the scale where the gravitational force exerted on them is comparable to the magnitude of these mentioned surface effects, pick-and-place begins to fail as a high precision, high volume process [18, 19]. Aside from stiction limitations, ultra-thin dice are so delicate that the down force of the placement nozzle often cracks the die

when it is either picked from the carrier tape or placed on the substrate [13]. Additionally, as the scale of dice continues to reduce, the nozzle vacuum force alone begins to raise concern as it causes the thin and flexible semiconductor components to flex. Placement heads could conceivably be scaled and configured to approach an ultra-thin component with sufficient precision to pick it up without shattering it. However, due to the mentioned surface effects, when the nozzle is in close proximity to a component these forces can cause a component to "jump" to the nozzle before it is in position to pick it up. This effect can also be observed when a component is placed. Small aberrations of a component's position in either of those steps will lead to placement errors unacceptable for the fine pitch components required for flex substrate devices.

Though a single nozzle placement machine may have the precision to place extremely fine pitch components, its inability to place ultra-thin dice [13] and similar components at a rate sufficient for high throughput assembly (>10 components/sec) has led to the pursuit of other techniques.

2.2. Fluidic Self Assembly

A novel component placement scheme called Fluidic Self Assembly (FSA®) has emerged in recent years providing a totally new concept for placing small-scale bare dice and micro-electro-mechanical system (MEMS) devices. Alien Technology Corporation has used the 3D geometric shape matching technology for the purpose of assembling radio frequency identification (RFID) tags. In the context of its use for assembling bare dice, the process [20-22] begins with a conventionally prepared Si wafer with functional ICs fabricated on its surface. Next, the wafer surface is processed to form shaped dice, pyramidal for example, across the entire surface of the wafer. These dice are termed

NanoBlock® IC devices, or simply NanoBlock®s. The NanoBlock®s, which are generally fully functional ICs, are then released from the wafer surface and collected for use in the next step. The substrate, which the IC chips will be mounted on, is prepared by etching or micromachining receptor sites with shapes corresponding to the shapes of the NanoBlock®s. If a pyramidal shaped NanoBlock® were used, the receptor hole would be of the same shape so a NanoBlock® fits neatly in it. The NanoBlock®s are then added to and suspended in an inert liquid assembly solution. This solution is gently washed over the substrate with receptor holes and the suspended NanoBlock®s self-assemble into the substrate receptor holes. After washing over the substrate, the assembly solution containing components, which did not bind to receptor holes, is collected and recycled for subsequent assembly runs. The assembly solution contains such a large number of NanoBlock®s that reported results indicate FSA® is very effective at assembling small-scale components. According to [22], as small as 185x185x40 μm NanoBlock®s are assembled with overall yield of nearly 100%. After the assembly step, the substrate is removed from the solution and dried. A conformal coating is then applied over the substrate surface to retain the assembled components. Finally, via hole drilling provides access to the component terminals and a metallization process provides electrical contact to the component.

The finer details of component shapes, densities, profiles and assembly solution characteristics such as viscosity have been studied in detail [17, 22]. Fairly sophisticated schemes for self-assembly beyond simply 3D geometric shape matching have been investigated. Capillary (fluid driven), capillary (molten-solder driven), magnetic, electrophoretic, and dielectrophoretic forces have all been studied for the purposes of placing delicate micro scale components [17].

Alien Technology Corporation has reported a throughput of up to 2 million parts per hour [17]. However, it is not yet clear if the FSA® technique is cost effective and well suited for high volume, high precision assembly required for ultra-thin, small, flexible devices. The fluidic assembly process may not be suited for all applications, or the assembly of certain types of components. Complex multi-step assembly processes may not be suitable for FSA® and the flexibility of a more direct placement technique is likely advantageous for certain applications. As a result of the passive assembly process the possible orientations of a placed NanoBlock® mean that component I/Os must either be limited and/or have built-in redundancies to allow for all the possible placement orientations. More complex shapes can be applied to limit the placement orientations of a NanoBlock® however that reduces the efficiency of the FSA® process and ultimately negatively affects the cost of device assembly. This process has been investigated thoroughly at NDSU's CNSE, affording the conclusion that there is no practical way of FSA®-ing components with difference sizes and shapes, ergo, different functionalities. This limitation is why FSA® has only been used to date for assembling single chip devices, such as RFID tags.

Though FSA® is a novel solution to small scale component assembly, the most optimal process would allow for high volume individual component assembly with placement precision and accuracy sufficient for ultra-fine pitch multiple I/O components in a preselected orientation. This would eliminate the FSA® requirement of redundant or limited I/O components and would provide the opportunity for even smaller scale, lower cost devices.

Various methods, most of which are still in the early R&D phase, have been suggested in the literature to capitalize where other methods have limitations [1, 2, 6, 9, 13]. The ability to selectively place components in a fashion similar to a SMD placement machine with the delicacy, speed and precision sufficient for high throughput of ultra-thin Si bare wafers is still the ideal goal. The area of Laser Induced Forward Transfer proposes to do that and is discussed next.

2.3. Laser Induced Forward Transfer – Ablative and Thermal Release

The basic concept of the technique known as Laser Induced Forward Transfer (LIFT) begins with a laser-transparent carrier substrate, which has a sacrificial layer deposited on its surface. The components to be transferred are bonded to the sacrificial layer. Once ready for transfer, the sacrificial layer is heated or ablated by a laser pulse to generate gases that propel the component towards a receiving substrate placed in close proximity.

The use of a laser for the transfer and contactless placement of discrete MEMS components was first reported by Holmes and Saidam [23, 24]. Recently, LIFT has been applied to the transfer of semiconductor bare dice. Karlitskaya and coworkers have developed a simple model that predicts the fluence threshold for the release of 200 × 200 μm by 150 μm thick Si tiles adhesively attached to a sacrificial PVC tape [25]. In a subsequent study [26], the authors described similar experiments for laser transfer in two distinct modes – ablative and thermal releasing, using relatively long pulse infrared and green lasers. In a number of publications, Piqué and coworkers have reported LIFT of individual InGaN LED bare dice (250 × 350 μm) using a series of very low fluence UV laser pulses [27] as well as a single-pulse transfer of various electronic components (bare

dice and SMDs) with sizes ranging from 0.1 to over 6 mm^2 in area [28-30]. Recently, Sheats [31] has described a process in which, in order to release the die, the release layer is heated up to a temperature of 100-150 ^oC by optically irradiating it with an intensity similar to that used in optical lithography. Although this process does not use a laser, it is very similar in nature to the thermal releasing process described by Karlitskaya *et al* [26].

The ablative releasing method has been found to provide highly unpredictable component transfers and results in a local system which behaves closely to a "confined ablation" configuration [32-34]. At the instant the sacrificial layer is heated by a laser it vaporizes. The vaporized materials are confined between the carrier substrate and the bonded component on its surface. The rapidly expanding localized plume of vaporized material projects the transfer component to the adjacent receiving substrate. By the nature of gas dynamics, the use of a relatively low density gas to push a higher density component such as a semiconductor die is highly sensitive to initial conditions. Small variations in the heat absorption mechanism, irregularities in the sacrificial layer thickness and homogeneity, presence of contamination as well as time based variations in the profile of the laser beam used for ablating the sacrificial layer all contribute to the ablative release process being highly unstable and the results highly unpredictable [23, 24]. Additionally, transfer velocities of components with this approach raise concern regarding the ability of components to land safely on a receiving substrate without sustaining damage [23]. Depending on the type of component being transferred, the sacrificial layer in the ablative releasing method may be configured so that it absorbs or transmits the laser irradiation at the wavelength of the transferring laser. This distinction determines whether absorption on the surface of the component heats the sacrificial layer to the point of vaporization or if the

absorption of the laser energy by the sacrificial layer serves as the heating mechanism. When a semiconductor component is transferred with a sacrificial layer which is not absorbing at the laser wavelength, small configuration variations will lead to drastically different heating conditions between subsequent transfers as a result of the nonlinear absorption of semiconductor materials at many wavelengths [25, 26]. However, this effect can be tempered by carefully selecting the laser wavelength used [26].

The thermal release LIFT technique developed by Karlitskaya *et al.* [26] is intended to address the transfer volatility and unpredictability observed in the ablative transfer process. Under a thermal releasing configuration the component to be transferred is prepared in the same way as the ablative releasing sample; however, the sacrificial layer behaves in a different manner. In this case, the sacrificial layer is heated slowly with laser fluences significantly lower than those used in an ablative release. Like the ablative approach, in most cases, the thermal release still relies upon the laser energy being absorbed by the semiconductor component to be transferred. The resulting process includes a more gradual heating of the sacrificial layer and provides for a less volatile and more predictable transfer process. The authors reported successful transfers of 300 × 300 μm by 130 μm thick Si tiles utilizing the thermal releasing process. Reportedly, 95% of these transfers occurred within a release angle of 9 degrees, which corresponds to a placement accuracy of ±35 μm assuming a 195 μm transfer gap is used. Note that these release angles were measured without the presence of a close proximity receiving substrate. These results were achieved with a flat top, frequency doubled Nd:YAG laser which reduces the nonlinear absorption at the semiconductor surface. Furthermore, the thermal releasing transfer velocities have been shown to be significantly less than transfers of the ablative

nature. This will be required to ensure not only successful component placement but more critically, the placement of a component that is functional once positioned. Though the thermal releasing LIFT approach shows potential and the reported die release angles indicate the possibility of very good transfer precision, to the best knowledge of the author, there has not yet been a report of successful laser transfer of an electronic component, such as a bare die, to an exact location on a circuit substrate, and which is functional after the transfer.

Moving forward, the community's focus for applying these techniques should ultimately be focused on a particular LIFT technique's precision and accuracy of placement, and ability to transfer the die to the receiving substrate without degrading its integrity. Considering these factors, the ideal LIFT technique will place components:

(i) smaller and thinner than what pick and place is capable of.

(ii) at a preselected, exact location and orientation.

(iii) without exceeding their heating damage threshold.

(iv) with energy below that which would cause mechanical damage during either positive or negative transfer accelerations.

(v) with a throughput capable of high volume manufacturing (>10 components/sec).

3. THE *tm*SLADT PROCESS

The major problem with the existing LIFT techniques is the accuracy and precision of placement. The experimental results indicate that projecting a component with an ablated plume of material makes it nearly impossible to accurately place it in the desired location. The major disadvantage of the ablative laser release, therefore, is the seemingly stochastic nature of the release dynamics and flight instability that makes achieving any consistency in the component placement accuracy virtually impossible. On the other hand, the thermal release method may not be suitable for small size components because the gravity force alone this method relies upon for the actual component transfer may not be sufficient enough to overcome the surface forces of attraction and release the object.

The results of the LIFT technique depend to a great extent on the layer which bonds the material to be transferred to the releasing substrate, known as the dynamic releasing layer (DRL). Most of the reported results rely on a single-layer DRL. Multi-layer configurations of the DRL were described in the patent literature [35] but it is not clear if these methods were ever realized for component transfer. In all these cases the absorbed laser energy causes a total or partial vaporization of the DRL. The kinetic energy of the vaporized material is then utilized to carry out the actual component transfer with all the negative consequences discussed in the previous section. The problems can be alleviated if the rapidly expanding gas is excluded from the actual transfer. Instead, the gas resulting from the laser ablation can be used to create a blister in the DRL that in turn will serve as a mechanical actuator to gently push the transfer components towards the receiving substrate. This approach, henceforth referred to as the Thermo-Mechanical Selective Laser Assisted Die Transfer process (*tm*SLADT – pronounced 'T'-'M'-SLAD), was adopted by the Laser

Enabled Advanced Packaging (LEAP) group at CNSE after observations in our initial experiments in which the DRL was a single layer of in-house developed material that would create a blister and at the same time soften enough to release the component (Figure) [36].

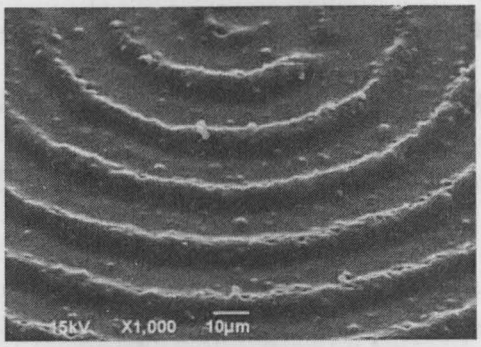

Figure . Thermo-mechanical response of DRL when irradiated with a scanning laser beam in a spiral pattern [36].

The absorbed laser energy ablates only the thin absorption region of the DRL leaving the rest of the layer intact. The confined gas exerts a force on the surrounding structure (non-vaporized portion of the film). When the pressure inside the blister generates stress in the surrounding layer that exceeds its yield strength, it starts to deform plastically and a blister forms. The pressure of the heated, expanding gas drops as the volume of the blister increases until steady state equilibrium is reached. There clearly exists a delicate balance, in terms of absorbed laser energy, absorbing layer thickness and material properties, which dictates whether or not a blister forms, the rate of blister formation, the size of the blister, and finally, whether or not the blister ruptures. Since the blister-actuator is fully enclosed, the hot gaseous environment experienced during the ablative LIFT and arguably, to a degree, the thermal LIFT process, is eliminated. In addition, the nonlinear absorption exhibited in semiconductors materials is now removed from the process, which should provide a more repeatable transfer process.

In a similar approach but for a different application, a recent study published by a group at Princeton University details the nature of enclosed blister formation in spin coated liquid polyimide DRL when irradiated by a UV laser [37]. The Princeton study focuses on the application of this process for purposes of ink printing and even for biomedical purposes. The DRL in this case is comprised of a 100nm – 10 μm polyimide layer which has a relatively shallow UV absorption depth of 0.2 – 0.5 μm [38].

The single-layer DRL configuration proved to be very sensitive to the properties of the blister/release layer. Three types of material properties had to be precisely controlled for a single-layer DRL to work: laser absorption, mechanical properties at elevated temperatures, and adhesive properties. Consequently, the concept of two-part DRL configuration was developed and implemented in which the first layer, adjacent to the glass carrier, will provide the blister mechanism and the second layer will be used to bond the transfer component (Figure). The dual-layer DRL configuration allows for uniquely formulating the bonding layer's adhesive strength while causing a minimal, or no, change to the dynamics of blister formation in the underlying absorbing/actuating layer.

Before exploring the finer details of DRL configuration for *tm*SLADT, an overview of the entire transfer process from start to finish is provided. The discrete components used in this study were blank silicon tiles. One would not expect the transfer dynamics of a functional silicon-based IC to differ significantly from a silicon tile with the same or nearly the same dimensions. The samples are prepared beginning with a polished fused silica substrate, which has relatively high UV transmission compared to other glasses. A polyimide layer is first spincoated and cured, upon which a PSA layer is spincoated and cured. Next, the thinned, 65 μm thick, silicon wafer is bonded to the PSA layer and the

wafer is diced with a laser (355 nm for this study). The wafer dicing can also be carried out by diamond sawing. After dicing, the sample preparation for individual tile transfers is finished. The transfer gap (separation between releasing and receiving substrates) is set accordingly and the DRL is irradiated with UV laser pulses in the appropriate location on the substrate polyimide interface to create the blisters-actuators which move the selected tiles or dice from the releasing to receiving substrate.

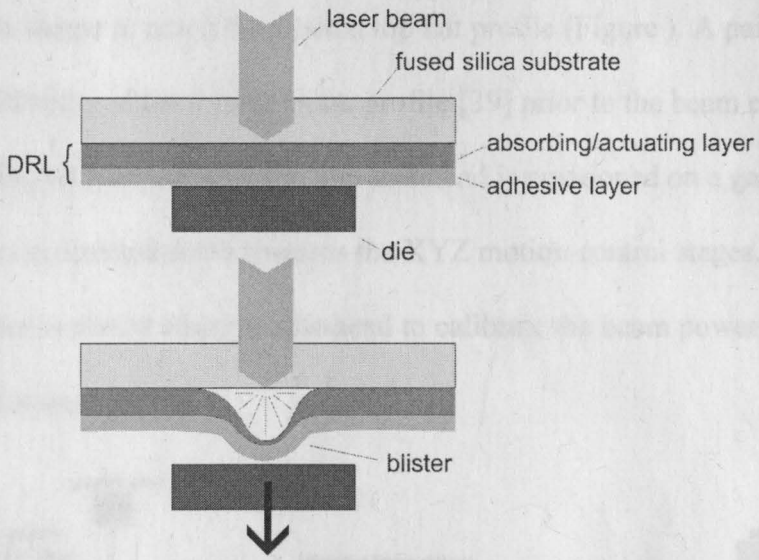

Figure . A schematic illustrating the principles of *tm*SLADT. DRL absorbs the laser pulse with energy below the blister rupture threshold of absorbing layer. This contains the gasses generated during absorption and provides an actuator mechanism to transfer the discrete component.

4. EXPERIMENTAL SETUP

The primary components of the *tm*SLADT experimental setup used for this study are illustrated in Figure . The setup begins with a Spectra Physics HIPPO Nd:YVO_4 laser where its third harmonic (355 nm) beam passes through a half wave plate dichroic polarizer variable attenuator. The waveplate is mounted in a rotation stage and a LabView® interface is used to control its angular position. Next, the beam is expanded and then passes through a refractive beam shaper to attain the desired top hat profile (Figure). A pair of relay lenses enhances the uniformity of the top hat beam profile [39] prior to the beam entering the laser scanhead (SCANLAB Hurry*SCAN*® *II*). The scanhead is positioned on a gantry mount and the scanned beam is directed down towards the XYZ motion control stages. Prior to each use, a power meter is placed after the scanhead to calibrate the beam power versus waveplate position on the sample.

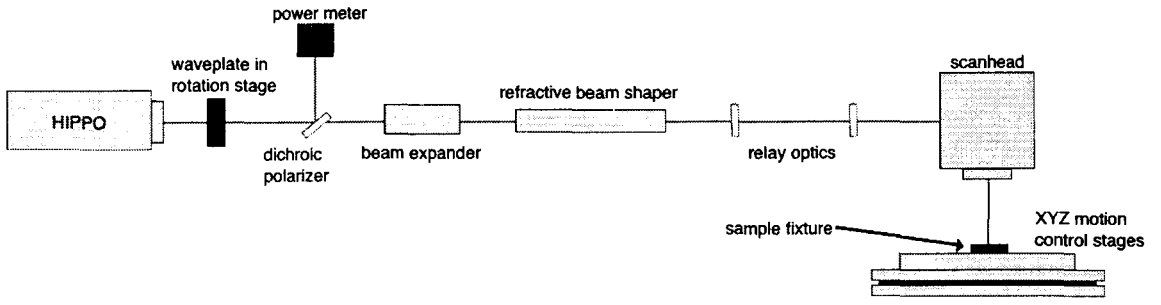

Figure . *tm*SLADT experimental setup.

The *tm*SLADT sample is placed on the stages and the sample position is set, along the axis of the beam, so the beam waist is in the same plane as the polyimide layer of the sample. Inspection of laser scribe lines on a Si wafer indicates a scanned flat top beam waist diameter of 10 μm is achieved with this setup.

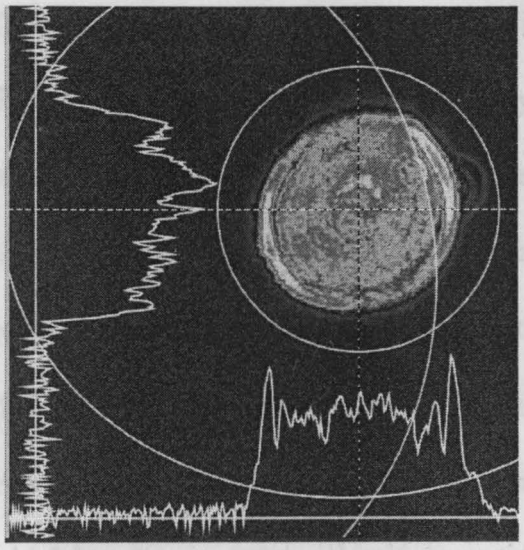

Figure . Laser beam top hat profile used for wafer dicing and *tm*SLADT. This profile was captured after beam exits the scanhead, before the waist.

5. DRL CONFIGURATION AND *tm*SLADT SAMPLE PREPARATION

The addition of a PSA on top of the absorbing/actuating layer introduces new factors to the process. First, the thickness of the PSA layer must be less than that of the absorbing/actuating layer. Experimentation showed a 4 μm thick layer of polyimide with no PSA overcoat would generate single pulse enclosed blisters with heights in the 15-20 μm range (size of static blister long after formation, actual blister displacement may be greater than that during formation due to the inertia of the expanding film). With the addition of a PSA layer, which has its own unique elastic properties, on top of the polyimide, the dynamics of blister formation should change. Considering this, the PSA layer must be much thinner than the underlying polyimide layer. Experimentation has indicated the thickness of the PSA layer should be no more than 25% of the polyimide layer, though this is an empirical benchmark. A PSA layer of greater thickness inhibits blister formation of sufficient height to induce component transfer.

The PSA must be formulated so that its adhesive strength is sufficient to hold the wafer securely on the releasing substrate during processing and laser dicing but not be so excessively tacky that it inhibits the components' release once the polyimide blister forms. This formulation was identified after a series of transfer attempts with different PSA formulations, which produced the following observations. First, each formulation had a unique spincoating curve. This led to many samples being created with an excessively thick layer, which had no chance of allowing tile transfer. Second, the elastic properties of a PSA are unique to its specific formulation. Even if a new formulation with an acceptable adhesive strength is created, the elastic properties may have changed simultaneously with the adhesion in such a way that the blister formation dynamics are changed. For example,

this study has found that relatively weak adhesion strength is needed for this process. Most PSA formulations, which provided desirable *tm*SLADT performance, were 'drier'. However, drier films of this type tend to also be less elastic. As we iteratively moved towards drier formulations the PSA also restricted the expansion of the polyimide blisters. These factors must all be balanced in order for successful transfers to occur and is the reason the PSA layer must be relatively thin compared to the underlying polyimide layer. The formulation for the PSA used to achieve the results reported in this study is listed in Table .

Material	Weight - %	Material Supplier
IRGACURE® 2022	2	BASF Resins
Urethane acrylate - BR 3741 AB	5	Bomar Specialties Company
Trifunctional urethane acrylate - CN929	10	Sartomer USA
1,6 hexanediol diacrylate - SR238B	43	Sartomer USA
Ethoxylated (3) trimethylolpropane triacrylate - SR454	40	Sartomer USA

Table . PSA formulation by weight used for the reported *tm*SLADT results. All materials used unaltered from suppliers.

Considering the sensitivity to initial conditions of the LIFT process, sample preparation must be done with great care and detail to ensure subsequent sample polyimide and PSA layers are as near to being identical as possible. Variations have a negative effect on transfer precision and rate. With this in mind, DRL formulating, deposition and wafer bonding to the DRL were performed in a class 100 clean room environment when possible. To begin, a 3 inch diameter by $1/16^{th}$ inch thick polished fused silica substrate was used as the carrier or releasing substrate upon which the HD MicroSystems™ PI2525 liquid polyimide was deposited without modification from the supplier. The polyimide thickness

of 4 μm was achieved by a two-step spin cycle. First, a 500-rpm spin was run for 10 seconds followed by a 5000 rpm spin for 40 seconds. After deposition, the spin coated liquid polyimide was soft-baked at 120°C for 30 minutes followed by a 30-minute ramp to 350°C for a final 30-minute hard bake.

Once the polyimide was cooled to room temperature the PSA was diluted 50% by weight with methyl isobutyl ketone (MIBK) and deposited with a two-cycle spin recipe. The first cycle was 500 rpm for 3 seconds followed by a 4000 rpm cycle for 50 seconds. This provided a uniform PSA layer, which was no more than 1 μm thick. It was then UV lamp cured at 1180 mW/cm^2 for 1 minute. Next, the thinned 65 μm Si wafer was bonded to the substrate by gently placing it on the PSA. Under ideal circumstances the weight of the wafer provides sufficient pressure for adequate bonding to the PSA. However, impurities in either the polyimide or PSA layers will inhibit the bonding process. If contamination is present, complete bonding may require delicate pressure on the portions of the wafer that are not in contact with the PSA. Note that this action can cause variations in the bonding adhesion as well as the thickness of the PSA, both of which lead to different conditions for the eventual transfer process. Considering the sensitivity of the process to these small changes a more suitable option for improving the bonded area of the placed wafer is to place the sample in vacuum.

After the wafer bonding process was complete, the sample was diced into 680 × 680 μm tiles. This was done via laser ablation along the streets of the bonded wafer with the same 355 nm HIPPO laser used for the transfer process itself, however, with a different repetition rate and pulse energy configuration. Depending on the sensitivity of the diced components to debris generated during dicing, the wafer may be spincoated with a thin

protective coating. This allows the recast Si material and the residual ablation debris to land on top of the thin photoresist layer that is subsequently stripped by a short solvent bath (Figure).

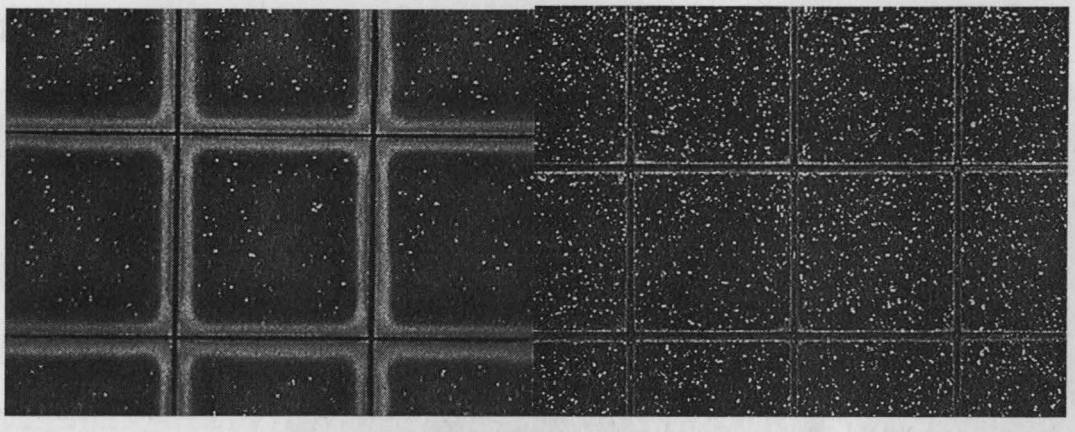

Figure . Dark field micrograph depicting the use of photoresist as a protective coating during Si wafer dicing. Image on left shows the debris adjacent to lased diced streets. Image on right is the same sample after photoresist was stripped and debris is no longer present.

However, for the results reported in the next section a protective coating was not used. After singulation was complete, the sample was inspected via a backlit optical microscope to ensure complete dicing was achieved. In some cases nearly complete dicing can occur but small tabs of Si remain intact across the diced streets, which inhibit the transfer process. Also, minor charring of the polyimide layer does at times occur along the wafer streets as well as pitting of the fused silica substrate causing refraction of the microscope backlight. These factors should not be confused with the presence of a tab between components when inspecting. Once the sample was fully diced, it was mounted in the fixture used for laser transfer. The fixture seen in Figure and Figure has a machined lip of 260 μm thickness, which serves to space the receiving and releasing substrates from each other (use of shims or any other physical contact between the two substrates is not required but simplified the setup). The releasing substrate was placed on top of the receiving

substrate with the DRL and wafer sample facing down. Prior to mounting the receiving substrate in the fixture it was spincoated with a PSA and cured in order to catch the transferred tiles. Since the average thickness of the wafer used in these samples was 65 μm thick, the transfer gap was 195 μm.

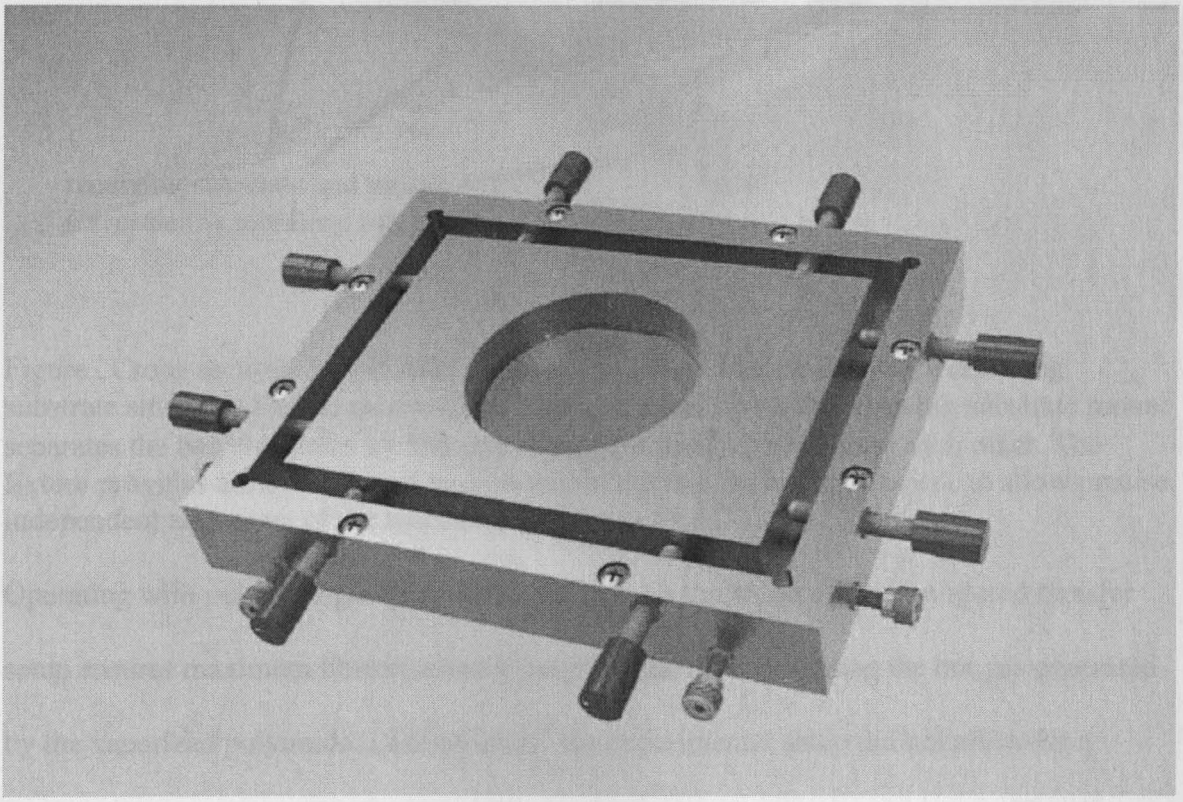

Figure . Sample fixture used to establish the *tm*SLADT transfer gap and position the releasing and receiving substrates relative to each other.

Once the substrates were mounted, the fixture was positioned under the scanhead (Figure) and the tiles awaited laser transfer. Based on characterization experiments, the rupture threshold of the DRL configuration with the 10 μm flat top beam was near 8 μJ. However, the presence of an object or material on the DRL surface increases this rupture threshold slightly as some of the energy is coupled to the transferred object in the form of kinetic energy.

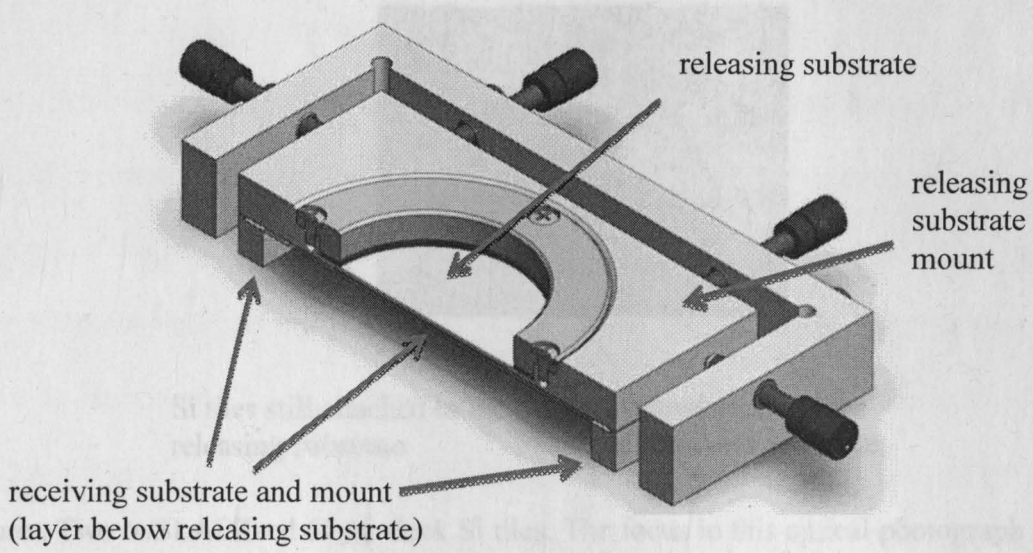

Figure . Cross-section of *tm*SLADT fixture. The internal block shows the releasing substrate sitting on top the receiving substrate. A small lip on the releasing substrate mount separates the two substrates by 195 μm, which are free to glide across each other. The fixture provides a small range of motion within a plane, including rotation, to allow precise independent alignment of the two substrates for *tm*SLADT.

Operating with pulse energies just below the rupture threshold of the configured transfer setup ensures maximum blister-actuator height while still containing the hot gas generated by the vaporized polyimide. Limitations of the experimental setup did not allow for a single pulse transfer mode. Consequently, a simple circular pattern was scanned on the back side of the tile which was selected for transfer. A scan speed that allowed for subsequent laser pulses to hit the DRL with nearly overlapping edges provided a continuous blister along the pattern of the laser scan. Other scan patterns where multiple locations on the substrate would be activated at the same time, each with an individual pulse, may be more ideal. Figure illustrates a typical result from the *tm*SLADT process.

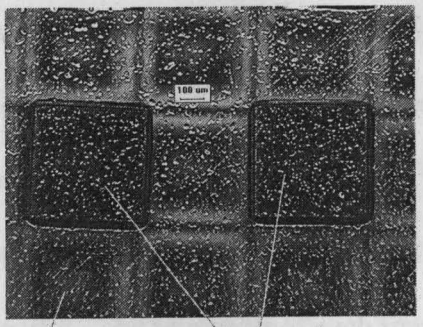

Si tiles still attached to the releasing substrate

Laser-transferred Si tiles on the receiving substrate

Figure . Two *tm*SLADT-ed 65um thick Si tiles. The focus in this optical photograph is on the receiving substrate. The releasing substrate, from where the tiles were transferred, is in the background.

6. DATA COLLECTION METHODS

Transfer precision and accuracy and transfer rate were recorded to evaluate the *tm*SLADT process. The tiles transferred to collect these statistics were not adjacent or diagonal on the releasing substrate (Figure) to limit possible DRL changes due to heating when a transfer was performed nearby. The precision of each transfer contains two data points as depicted in Figure , one each for radial displacement and angular rotation of the tile from its original position on the releasing substrate. This was recorded, before separating the releasing and receiving substrates after transfer, by looking through the releasing substrate via an optical microscope. A transferred tile's position was determined by observing its radial translation and angular rotation relative to the diced array, which remained on the releasing substrate.

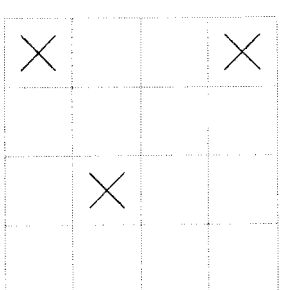

Figure . Map of a diced Si wafer. Typical spacing of transferred tiles is depicted with an "x".

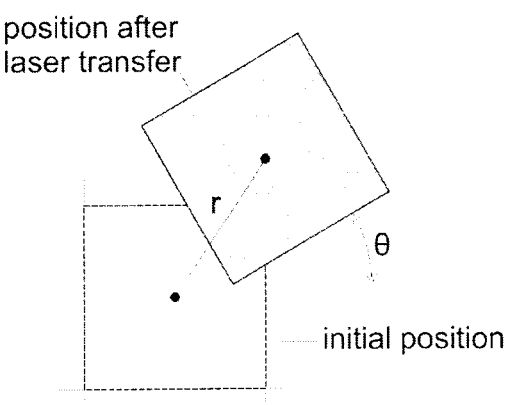

Figure . The radial displacement (r) and rotation (θ) of transferred tiles were used to evaluate the transfer precision of the tmSLADT process.

The optical microscope image capture software used to view the transferred tiles has built in on-screen measurement tools which are capable of both distance and angular measurements. These functions were first calibrated by measuring a series of known

distances and angles and then used to compare the placement position of transferred tiles to the tiles which surrounded them prior to the transfer as seen in Figure .

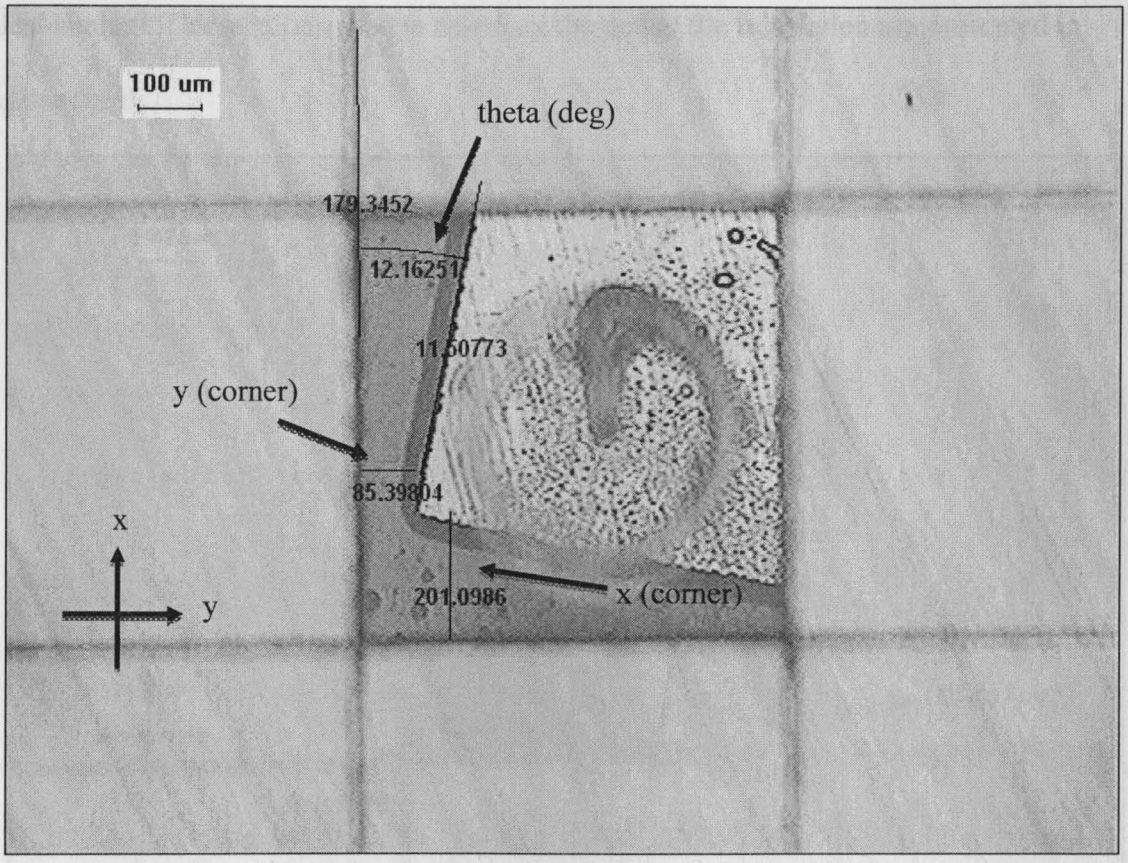

Figure . The microscope image capture measurement tools were used to capture the landing positions of the transferred tiles. Values are displayed in μm and degrees. The circular blister-actuator is slightly out of focus and above the transferred tile. The large transfer displacement and rotation of this transferred tile illustrate the measurement method well but this particular transfer has a larger translation and rotation than most. The reason was that the laser scanning pattern was not positioned precisely with respect to the center of the transferred tile.

The radial displacement value represents the distance the center of a tile moved from its pre-transfer position. However, the direct measurement of this value was not possible since the exact centers of the tiles were not marked. In order to determine the displacement of the centers of tiles, the x and y axis coordinates of a corner of the tiles were measured along with their rotation. In order to ensure consistency between tiles, the reference frame was always oriented so that the tiles' rotation was a positive angle

measured from the x-axis as seen in Figure . The combination of these two data points, along with the known dimensions of the tiles, allow for the displacement calculation of the tiles' centers. The relations used to calculate the actual tile translation are presented in Appendix B.

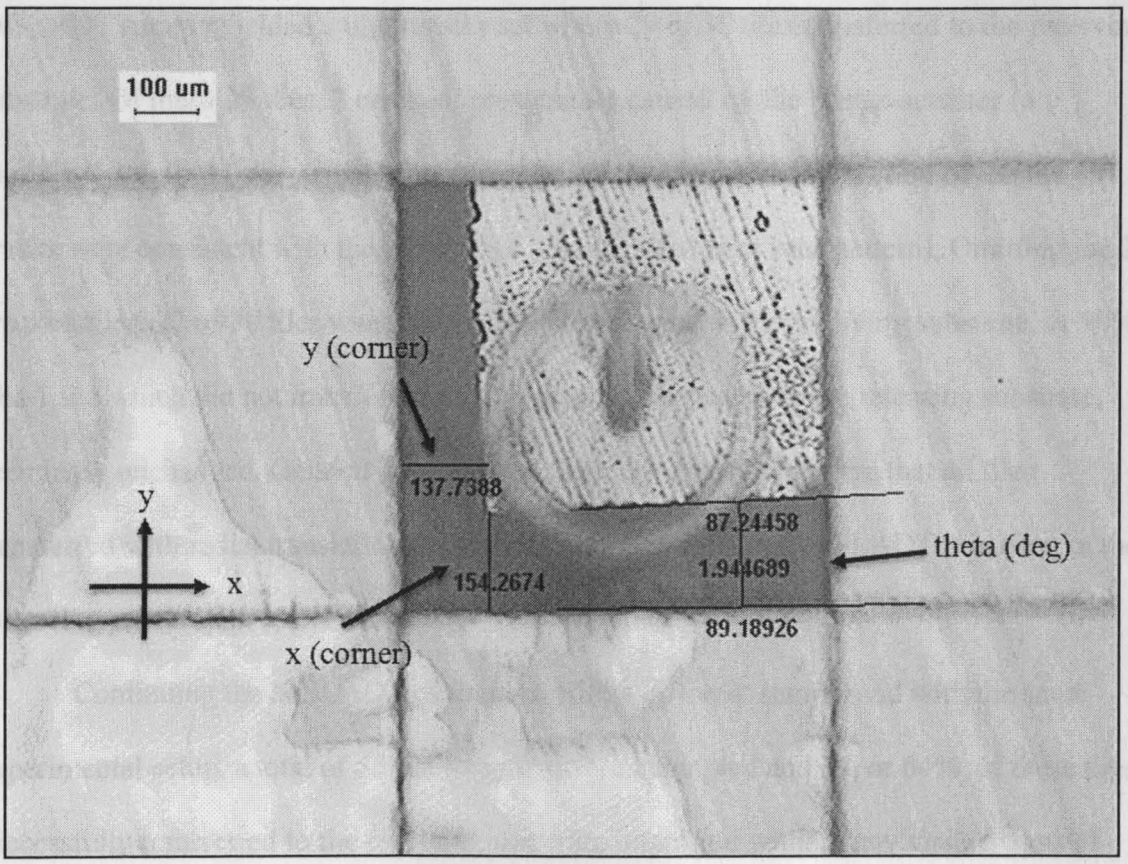

Figure . The reference frame used for measuring the transferred tiles was rotated depending on the landing position of the transferred tile.

7. RESULTS AND DISCUSSION

Initial efforts of *tm*SLADT study focused simply on tile transfer rate as the PSA formulation was iteratively modified to provide optimal adhesive and elastic properties. In these activities a wide range of transfer rates were observed. Most notably, an earlier *tm*SLADT sample yielded a tile transfer set where 29 of 30 tiles transferred to the receiving substrate. Of these 29 tiles, 2 cracked, presumably caused by the blister-actuator (a modified circular blister-actuator was scanned by the laser and the position of the tile cracks were consistent with the position of a 'tail' in the laser scan pattern). Omitting the 2 cracked tiles, 27 of 30 tiles were successfully transferred to the receiving substrate, or 90%. The 1 tile which did not transfer after the laser-scan remained on the releasing substrate, seemingly unchanged. General observations from the experiment were that all tiles transferred with radial translations consistent with the measured *tm*SLADT precision in the following paragraph.

Continuing the *tm*SLADT evaluation with a different sample and with the same experimental setup, a total of 55 tile transfers were attempted and 35, or 64%, of these tiles successfully transferred to the receiving substrate intact and without any visible signs of cracking or other damage. The 20 tiles which did not transfer after the laser-scan remained on the releasing substrate, seemingly unchanged. Transfer rate is highly dependent upon sample preparation and is not yet well understood. Also, three transfer outliers were removed (see Appendix B), leaving 32 transferred tiles to provide the accuracy and precision data. The measured tile radial displacement mean, median and standard deviation were 61.2, 50.0 and 46.3 μm, respectively. Figure is a radial displacement scatter plot for the 32 tile transfer set with a 195 μm transfer gap. The rotational displacement mean,

median and standard deviation were 4.2, 3.5 and 4.1 degrees, respectively. Considering the 195 μm transfer gap used for this experiment, the release angle mean, median and standard deviations were 17.0, 14.0 and 13.1 degrees, respectively. The release angle values were calculated assuming the transferred tiles traveled along a straight path between the releasing and landing positions.

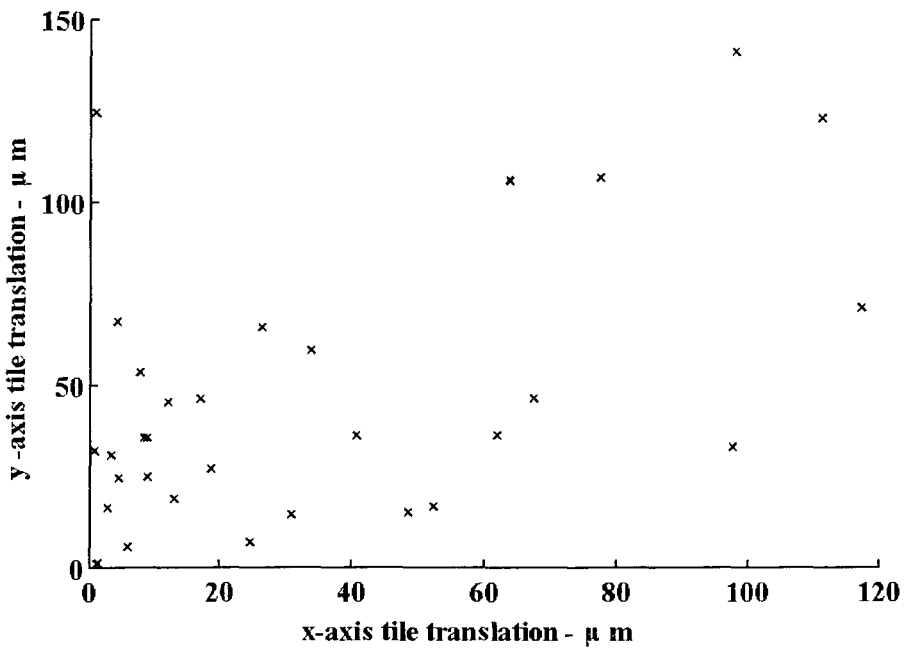

Figure . XY scatter plot of transferred Si tiles depicting lateral displacement in μm from tiles' release positions.

The *tm*SLADT transfer precision results are comparable to the thermal LIFT results previously published [26]. Those results measured release angles and only speculated on the landing positions of the transferred components. It is likely that flight dynamics of transferred components are changed by the close proximity of the receiving layer to the releasing layer. Experiments should be done with various transfer gaps to determine if the flight paths of transferred tiles are in fact straight between the release and landing positions. Also, further investigation will be done to determine the most likely differences

between tiles that successfully transfer and those that do not. In the course of this research transfer rates as high as 90% and as low as 0% have been observed. These wildly varying outcomes are attributed to the configuration sensitivity of the DRL required to optimize the *tm*SLADT process.

8. CONCLUSION

The use of lasers offers a unique opportunity to place small-size individual electronic components, including ultra-thin semiconductor functional dice, on substrates that may not be compatible with traditional pick-and-place equipment. Currently, it is the most promising, if not the only feasible method for high volume assembly of small size, ultra-thin semiconductor bare dice, essential for the next generation of mass produced high component density miniature electronic components. These components can be easily damaged during standard pick-and-place releasing using a metal placement nozzle. Due to dominating surface forces at the scale of ultra-thin bare dice, component placement with sufficient accuracy and precision required for ultra-fine pitch components may not even be achievable. Additionally, in comparison to FSA® techniques, the ability to selectively place individual ultra-thin bare dice will most certainly have advantages for certain packaging applications.

The laser release is a contactless process and, if properly controlled, is expected to provide the means for assembling ultra-thin semiconductor components required for flex substrate electronics packages. As such, this method can be described as an enabling technology providing capabilities not available today. The results from the proof of concept experiments presented in this paper demonstrate *tm*SLADT's ability to transfer 680 × 680 μm and 65 μm thinned Si tiles across a 195 μm transfer gap. In these experiment, a transfer rate as high as 90% was observed while median tile transfer rotation and release angles were 3.5 and 14 degrees respectively. The optimization and implementation of this capability on an industrial scale should enable cheap, flexible electronic devices. The *tm*SLADT process developed at the NDSU Center for Nanoscale Science and Engineering

is a unique contribution to this pursuit and provides several advantages over other LIFT techniques proposed to date. It has the potential to enable the assembly of the technological capabilities users of tomorrow will demand while reducing the resources consumed per component and ultimately should result in a cost reduction measured not in percents but in orders of magnitude.

REFERENCES

[1] C. Banda, *et al.*, "Flip chip assembly of thinned silicon die on flex substrates," *Electronics Packaging Manufacturing, IEEE Transactions on,* vol. 31, pp. 1-8, 2008.

[2] K. Y. Chen, *et al.*, "Ultra-thin electronic device package," *Advanced Packaging, IEEE Transactions on,* vol. 23, pp. 22-26, 2002.

[3] W. Christiaens, *et al.*, "Embedding and assembly of ultrathin chips in multilayer flex boards," *Circuit World,* vol. 34, pp. 3-8, 2008.

[4] B. Holland, *et al.*, "Ultra-thin, flexible electronics," in *Electronic Components and Technology Conference, 2008. ECTC 2008. 58th*, 2008, pp. 1110-1116.

[5] Z. Hou, "Integration of thin flip chip in liquid crystal polymer based flex," Doctor of Philosophy, Electrical and Computer Engineering, Auburn University, Auburn, Alabama, 2006.

[6] B. Pahl, *et al.*, "Ultrathin assemblies on flexible substrates," in *Proc. of 7th Electronic Packaging Technology Conference*, Singapore, 2005, p. 6.

[7] E. Parton, *et al.*, "Embedded chips redefine miniaturization," *Printed Circuit Design & Fabrication,* vol. 26, p. 37, 2009.

[8] T. Zhang, *et al.*, "Flexible Electronics: Thin Silicon Die on Flexible Substrates," *Electronics Packaging Manufacturing, IEEE Transactions on,* vol. 32, pp. 291-300, 2009.

[9] J. W. Balde, *Foldable Flex and Thinned Silicon multichip packaging technology*: Springer, 2003.

[10] "Introduction to Semiconductor Technology - AN900 Application Note" STMicroelectronics, Inc., 2000.

[11] V. Marinov and S. Bhattacharya, "High-Density PTF-Inlaid Traces on Flexible Substrates," presented at the Advanced Technology Workshop on Printed Devices & Applications, Orlando, FL, 2009.

[12] A. Piqué, *et al.*, "Embedding electronic circuits by laser direct-write," *Microelectronic Engineering,* vol. 83, pp. 2527-2533, 2006.

[13] M. Feil, *et al.*, "The challenge of ultra thin chip assembly," in *Electronic Components and Technology Conference, 2004. Proceedings. 54th*, 2004, pp. 35-40 Vol.1.

[14] M. Ayob and G. Kendall, "The optimisation of the single surface mount device placement machine in printed circuit board assembly: a survey," *International Journal of Systems Science,* vol. 40, pp. 553-569, 2009.

[15] W. Wang, *et al.*, "Optimization of high-speed multi-station SMT placement machines using evolutionary algorithms," *Electronics Packaging Manufacturing, IEEE Transactions on,* p. 10, 1999.

[16] K. Gilleo, *Area Array Packaging Processes*: McGraw-Hill Professional, 2003.

[17] M. Mastrangeli, *et al.*, "Self-assembly from milli- to nanoscales: methods and applications," *Journal of Micromechanics and Microengineering,* vol. 19, p. 37, 2009.

[18] F. Arai, *et al.*, "Adhesion forces reduction for micro manipulation based on micro physics," presented at the IEEE Workshop on Micro Electro Mechanical Systems, San Diego, CA, 1996.

[19] R. S. Fearing, "Survey of sticking effects for micro parts handling," in *International Conference on Intelligent Robots and Systems; human robot interatction and cooperative robots*, Pittsburgh, PA, 1995.
[20] "White Paper - Fluidic Self Assembly," Alien Technology Corp., 1999.
[21] J. S. Smith and H. J. Yeh, "Method for fabrication self-assembling microstructures," U.S. Patent, 1996.
[22] E. J. Snyder, *et al.*, "Fluidic self-assembly of semiconductor devices: a promising new method of mass-producing flexible circuitry," *Japanese Journal of Applied Physics,* vol. 41, pp. 4366-4369, 2002.
[23] A. Holmes, "Laser processes for MEMS manufacture," *RIKEN Review,* vol. 43, pp. 63-69, 2002.
[24] A. Holmes and S. Saidam, "Sacrificial layer process with laser-driven release for batchassembly operations," *Journal of Microelectromechanical Systems,* vol. 7, pp. 416-422, 1998.
[25] N. Karlitskaya, *et al.*, "Study of laser die release by Q-switched Nd: YAG laser pulses," in *High-Power Laser Ablation V* Taos, NM, 2004, pp. 935-943.
[26] N. Karlitskaya, *et al.*, "Laser propulsion of microelectronic components: releasing mechanism investigation," in *High-Power Laser Ablation VI*, Taos, NM, 2006, pp. 62612P 1-10.
[27] A. Piqué, Mathews, S. A., Pratap, B., and Auyeung, R. C "Laser forward transfer of semiconductor devices," in *Symposium on Laser Precision Microfabrication Conference*, Williamsburg VA, 2005.
[28] S. Mathews, *et al.*, "Use of Laser Direct-Write in Microelectronics Assembly," *JLMN-Journal of Laser Micro/Nanoengineering* vol. 2, pp. 103-107, 2007.
[29] A. Piqué, *et al.*, "Laser forward transfer of electronic and power generating materials," in *Laser Ablation and Its Applications*, C. Phipps, Ed.: Springer, 2007, pp. 339–373.
[30] A. Piqué, *et al.*, "Laser direct-write of embedded electronic components and circuits," in *Photon Processing in Microelectronics and Photonics IV* San Jose, CA, 2005, p. 223.
[31] J. R. Sheats, "Printing Silicon Integrated Circuits," in *Printed Electronics USA 2008*, San Jose, CA.
[32] R. Fabbro, *et al.*, "Physical study of laser-produced plasma in a confined geometry," *Journal of Applied Physics,* vol. 68, pp. 775-784, 1990.
[33] R. D. Griffin, *et al.*, "Interferometric studies of the pressure of a confined laser-heated plasma," *Journal of Applied Physics,* vol. 59, pp. 1968-1971, 1985.
[34] A. D. Zweig and T. F. Deutsch, "Shock waves generated by confined XeCl excimer laser ablation of polyimide," *Applied Physics B,* vol. 54, pp. 76-82, 1992.
[35] E. S. Handy, *et al.*, "Laser transfer article and method of making.," US Pat. 7,423,286, Filed Sep 7, 2004.
[36] S. S. Ahmad, *et al.*, "Cooperative Agreement DMEA H94003-08-2-0805: Electronics and Materials for Flexible Sensors and Transponders-I: Final Report," NDSU/CNSE, Fargo, 2009.
[37] M. S. Brown, *et al.*, "Time-resolved study of polyimide absorption layers for blister-actuated laser-induced forward transfer," *Journal of Applied Physics,* vol. 107, Apr 2010.

[38] J. H. Brannon, *et al.*, "Excimer laser etching of polyimide," *Journal of Applied Physics,* vol. 58, pp. 2036-2043, 1985.

[39] C. M. Jefferson and J. A. Hoffnagle, "Aspheric Laser Beam Reshaper Applications Guide," IBM Almaden Research Center.

[40] J. A. Hoffnagle and C. M. Jefferson, "Design and performance of a refractive optical system that converts a Gaussian to a flattop beam," *Applied Optics,* vol. 39, pp. 5488-5499, Oct 20 2000.

[41] B. R. Frieden, "Lossless conversion of a plane laser wave to a plane wave of uniform irradiance," *Applied Optics,* vol. 4, pp. 1400-1403, 1965.

[42] J. L. Kreuzer, "Coherent light optical system yielding an out-put beam of desired intensity distribution at a desire equiphase surface," U.S. Patent, 1969.

[43] W. Jiang, *et al.*, "Design and testing of a refractive reshaping system," in *Current Developments in Optical Design and Optical Engineering III*, 1993, pp. 64-75.

[44] P. W. Rhodes, *et al.*, "Refractive optical systems for irradiance redistribution of collimated radiation: their designs and analysis," *Applied Optics,* vol. 19, pp. 3545-3553, 1980.

[45] C. Wang and D. L. Shealy, "Design of gradient-index lens systems for laser beam reshaping," *Applied Optics,* vol. 32, pp. 4763-4769, 1993.

APPENDIX A: FLAT TOP BEAM SHAPING

A notable topic of interest not directly tied to the concept of advanced microelectronics packaging is the concept of laser beam shaping. Though, for the purposes of LIFT, beam shaping is a practice often employed and, as mentioned in the preceding text, was utilized in the development of *tm*SLADT. A vast majority of laser systems encountered in industrial and manufacturing settings are mode TEM_{00}, produced by a high-Q optical cavity. This type of profile is known as a Gaussian beam with a cross sectional or radial intensity profile proportional to $\exp(-2r^2/\omega_0^2)$. The r term represents the radial position within the beam cross section and the ω_0 term is known as the beam waist and describes the beam size. The unaltered Gaussian beam profile of the HIPPO laser used in this study is shown in Figure .

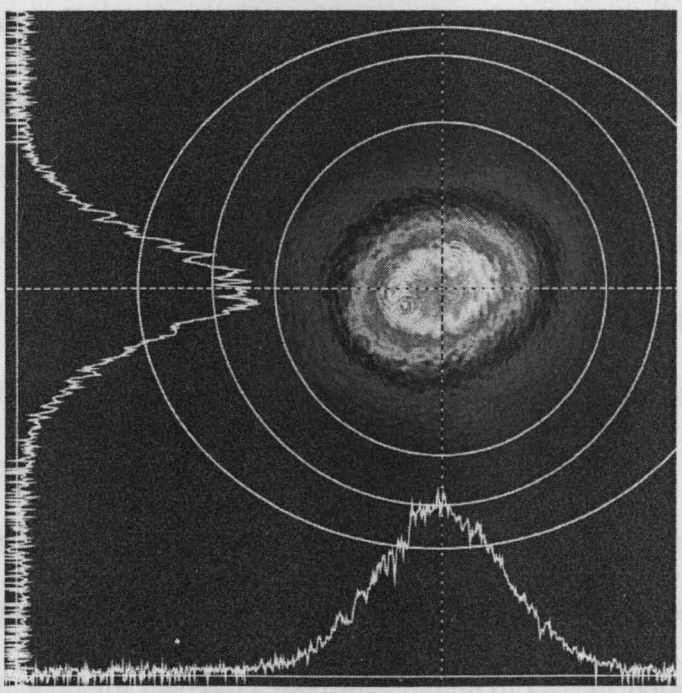

Figure . Gaussian beam profile of the HIPPO laser used in this study. A slightly elliptical shape is attributed to the mixing crystals and is also observed in the reshaped flat top beam seen in Figure .

Considering the many applications of laser systems, the Gaussian beam profile is often not the most desirable or effective distribution of laser energy. In laser etching, scribing, micromachining and many other materials processing applications, the ability to irradiate a surface with uniform intensity is generally advantageous and can simplify several parameters including scan patterns and power modulation. In situations where uniform laser beam irradiance is required, or advantageous, a simple solution is to expand the Gaussian beam and mask the peripheral areas of the beam where the intensity falls off from the peak. This will allow only the peak intensity of the beam profile to pass through to the area of interest. When the area of interest is small compared to the size of the expanded beam, nearly a uniform intensity profile can be achieved. Though this approach is suitable for some applications, it is inefficient because the mask blocks a large portion of the beam energy. The need for uniform irradiance in an area of interest combined with loss of beam energy as well as aperture diffraction effects when using a mask are the principal motivation for beam shaping.

The concept of beam shaping refers to the practice of redistributing the cross sectional energy of a laser beam. Depending on the specific needs of an application, different beam profiles may be advantageous. In the realm of beam shaping, a commonly sought after beam profile is the flat top (top hat) beam. It is aptly named because this process redistributes the laser beam energy uniformly across the cross section of the beam. Though other profiles may be achieved, the flat top beam shape is of particular interest for laser dicing of semiconductor materials, micromachining of various polymers and *tm*SLADT. The gradual radial dependent change in intensity of a Gaussian beam leads to melting as the intensity falls off near the beam edge where it no longer has sufficient

intensity to vaporize material in the area of interest. The flat top profile enables dicing and micromaching with greater precision and with better defined cuts than a Gaussian beam profile since the beam kerf has sharp intensity change at the edge of the beam.

Flat top beam shaping can be achieved in a number of ways [40], which include filters with radial dependent absorption profiles, diffractive elements in the form of holographic or binary optics, and reflective or refractive anamorphic optical systems. Each approach has its drawbacks. For example, radially varying absorption spatial filters still have significant energy losses and are limited to applications with relatively low beam energy. Diffractive elements require extremely sensitive spatial alignment and, due to the nature of diffractive optics, are only effective near a specific design wavelength. Holographic shaping schemes also have large energy losses, require extremely precise alignment for optimal performance and are also wavelength dependent. Reflective optics generally must be aligned off axis or beam obscuration will result. This often requires complex surfaces that can present fabrication challenges. The primary advantage of the refractive shaping approach is high efficiency. This approach was first described by Frieden [41], followed by Kreuzer [42] and later by Shealy and others[43-45]. The most basic concept utilizes a pair of aspheric lenses, one plano concave and the other plano convex positioned according to Figure . The collimated beam enters the first lens and is diverted from its center axis. As a result of using aspheric lenses the degree of ray divergence at the first lens is dependent on the radial position where the ray enters the optic. A ray directly on the center axis of the beam/lens will propagate though with no change in direction. A ray near the center axis of the lens will experience the greatest degree of divergence while a ray passing through the periphery of the lens will experience

relatively small divergence from its original path. Considering the energy profile of a Gaussian beam one can reason this scheme will redistribute the center portion of a Gaussian beam, which is most intense, to the edges of the aperture, where the entering beam is least intense. The second lens must be positioned at the point where the diverging rays, resulting from the Gaussian beam passing through the first lens, reach a uniform cross sectional density. At that point, the converging lens serves to recollimate the beam and provides for the desired plat top profile.

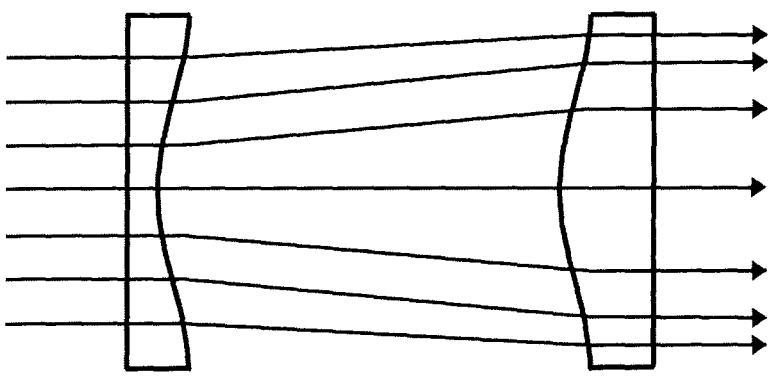

Figure . Ray trace of an aspheric-lens beam reshaping system.

The reshaping lens system used for the work discussed in this study is a commercial off-the-shelf system purchased from the Newport Corporation; model number GBS-UV-H, which is designed to operate in the wavelength range of 240-440nm. According to the manufacturer's specification, when the device is setup correctly, 99.7% of the input energy is present in the reshaped output beam. Hoffnagle and Jefferson present a review of the refractive reshaping concept as well as a thorough review of the implementation of the Newport reshaper where they detail the process of setting up and aligning the optical train for an optimum flat top laser beam [39, 40].

A considerable amount of time during this study was spent on the optical alignment of the experimental setup. Specifically, achieving the desired flat top beam profile used for

laser dicing and *tm*SLADT was especially time consuming. The basic beam shaper setup used for the work in this study is presented in Figure . The alignment and positioning of optics along the beam path are extremely crucial to shaping the beam to the desired profile. Small changes, caused by settling of optical mounts over the course of a day or two along with setup aberrations likely due to vibrations present in a table or even temperature changes within a setup contribute large enough changes in alignment to cause a noticeable change in the beam profile. In order to provide sufficient alignment adjustment, the beam expander and beam shaper were both mounted in their own 5-axis v-block mounts. Regular beam profiling at the beginning of every day the laser is used is crucial to ensuring one is operating with an optimum flat top beam profile. Nearly every day, small adjustments are required to the tilt, yaw or XY position of the beam shaper in order to ensure the beam energy is evenly distributed for an optimum flat top profile.

APPENDIX B: *tm*SLADT TRANSFER EVALUATION DATA

The following tables contain the data collected and used to provide the *tm*SLADT accuracy and precision statistics. The group statistics for all 35 tile transfers were first calculated. Then outliers were identified by exceeding a 2σ threshold in either the rotation or radial displacement categories. The group statistics were then recalculated for the 32 remaining tile transfers and were reported in the results section. The x_c and y_c values are the x and y coordinates of the selected corner of the transferred tile. The theta (deg) column was a direct measurement made with the microscope image capture software. This value was then converted to radians and displayed in the theta (rads) column. Utilizing the known dimensions of the transferred tiles, the x and y displacement of the center of the transferred tile from the xy origin of the measurement reference frame is listed in the x_d and y_d columns. Next, the actual displacement of the tiles' centers were calculated and listed in the Radial Disp. column by subtracting the xy coordinate of the tiles' pre-transfer position from the landing position. Finally, the $x_{trans.}$ and $y_{trans.}$ columns represent the coordinates of the transferred tiles' centers. These columns were used to generate the xy scatter plot presented in Figure . Figure and subsequent equations illustrate the geometry involved in calculating the position of the transferred tile. Table 4 is a record of the tile transfer attempts and successes organized by row of the diced sample used for the study.

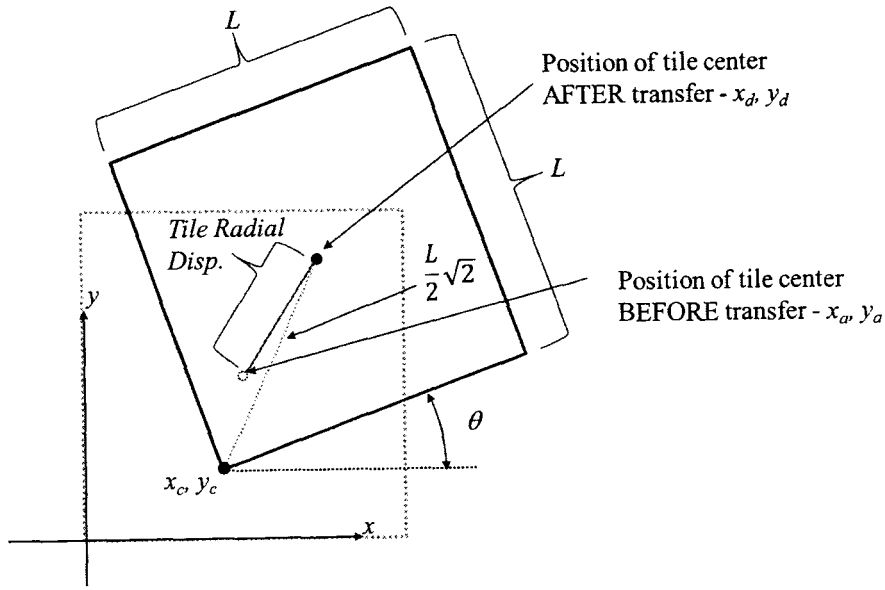

Figure . Illustration of geometry involved in calculating tile transfer radial displacement. The dotted line square represents the tile's position before transfer and the solid line square represents the position of the tile after it has been transferred to the receiving substrate.

$$x_a = \frac{L}{2} \quad y_a = \frac{L}{2}$$

$$x_d = \frac{L}{2}\sqrt{2}cos(\theta + 45^\circ) + x_c \qquad y_d = \frac{L}{2}\sqrt{2}sin(\theta + 45^\circ) + y_c$$

$$Radial\ Disp. = \sqrt{(x_d - x_a)^2 + (x_d - x_a)^2}$$

$$x_{trans.} = x_{disp.} - \frac{L}{2} \qquad y_{trans.} = y_{disp.} - \frac{L}{2}$$

Table . Tile radial displacement and rotation. All values, except angular measurements, are in μm.

	x_c	y_c	**theta (deg)**	**theta (rads)**	x_d	y_d	**Radial Disp.**	$x_{trans.}$	$y_{trans.}$
1	22	0	**4.49**	0.0784	320.56	349.45	**24.85**	4.44	24.45
2	46.8	88.15	**2.25**	0.0393	358.79	384.31	**68.26**	33.79	59.31
3	0	0	**0.18**	0.0031	323.98	326.02	**1.44**	1.02	1.02
4	2.75	24.79	**1.05**	0.0183	321.74	355.69	**30.86**	3.26	30.69
5	33.05	0	**3.42**	0.0597	338.08	343.81	**22.91**	13.08	18.81
6	112.95	126.72	**2.58**	0.0450	422.99	466.02	**171.72**	97.99	141.02
7	0	27.55	**1.43**	0.0250	316.79	360.56	**36.50**	8.21	35.56
8	35.81	27.55	**4.78**	0.0834	332.60	378.50	**54.04**	7.60	53.50
9	179.06	19.28	**10.08**	0.1759	442.16	396.15	**137.07**	117.16	71.15
10	22.04	41.32	**0.87**	0.0152	342.07	371.22	**49.27**	17.07	46.22
11	121.21	11.02	**4.03**	0.0703	422.57	358.06	**103.01**	97.57	33.06
12	123.96	55.1	**9.82**	0.1714	388.77	430.77	**123.50**	63.77	105.77
13	0	0	**1**	0.0175	319.28	330.62	**8.02**	5.72	5.62
14	0	13.77	**0.47**	0.0082	322.32	341.43	**16.64**	2.68	16.43
15	88.15	13.77	**10.08**	0.1759	351.25	390.64	**70.69**	26.25	65.64
16	68.86	-19.28	**12.94**	0.2258	312.83	370.24	**46.85**	12.17	45.24
17	0	0	**0.22**	0.0038	323.75	326.25	**1.76**	1.25	1.25
18	33.06	93.66	**5.7**	0.0995	324.17	449.33	**124.33**	0.83	124.33
19	82.64	-49.59	**15.88**	0.2772	306.31	351.93	**32.78**	18.69	26.93
20	49.59	14.04	**0.2**	0.0035	373.45	340.17	**50.77**	48.45	15.17
21	49.58	-30.3	**4.27**	0.0745	349.48	318.00	**25.46**	24.48	7.00
22	82.64	16.52	**3.55**	0.0620	386.89	361.02	**71.61**	61.89	36.02
23	-20	16.5	**3.55**	0.0620	284.25	361.00	**54.37**	40.75	36.00
24	93.66	22.04	**4.45**	0.0777	392.46	371.28	**81.81**	67.46	46.28
25	13.77	19.28	**2.27**	0.0396	325.64	356.90	**31.90**	0.64	31.90
26	88.15	96.42	**1.83**	0.0319	402.61	431.63	**131.88**	77.61	106.63
27	55.1	-8.26	**4.16**	0.0726	355.67	339.46	**33.91**	30.67	14.46
28	184.57	63.36	**11.8**	0.2059	436.24	447.95	**165.81**	111.24	122.95
29	8.26	63.36	**0.71**	0.0124	329.21	392.36	**67.49**	4.21	67.36
30	11.2	33.06	**0.43**	0.0075	333.75	360.49	**36.55**	8.75	35.49
31	35.81	0	**4.58**	0.0799	333.82	349.91	**26.43**	8.82	24.91
32	55.1	13.77	**0.49**	0.0086	377.31	341.54	**54.86**	52.31	16.54

Table . Tile radial displacement and rotation outliers.

	x_c	y_c	**theta (deg)**	**theta (rads)**	x_d	y_d	**Radial Disp.**	$x_{trans.}$	$y_{trans.}$
33	0	630	**13.6**	0.2373	239.47	1022.31	**702.53**	85.53	697.31
34	173.55	155.77	**39.98**	0.6977	213.77	613.63	**309.32**	111.23	288.63
35	275.48	123.96	**11.56**	0.2017	528.76	507.50	**273.54**	203.76	182.50

Table . Tile transfer rate.

Row	Attempts	Transfer	
1	7	4	
2	2	2	
3	6	5	
4	1	1	
5	5	3	
6	1	1	
7	5	1	
8	1	1	
9	3	2	
10	5	0	
11	4	3	
12	5	4	
13	4	3	
14	5	4	
15	1	1	**Transfer Rate**
	55	35	**64%**